

Machine-learning Based Screening of Lead-free Halide Double Perovskites for Photovoltaic Applications

Elisabetta Landini

*Fritz-Haber-Institut der Max-Planck-Gesellschaft, Faradayweg 4-6, D-14195 Berlin, Germany and
Chair for Theoretical Chemistry and Catalysis Research Center, Department of Chemistry,
Technische Universität München, Lichtenbergstr. 4, 85748 Garching, Germany*

Karsten Reuter

Fritz-Haber-Institut der Max-Planck-Gesellschaft, Faradayweg 4-6, D-14195 Berlin, Germany

Harald Oberhofer

*Chair for Theoretical Physics VII and Bavarian Center for Battery Technology (BayBatt),
University of Bayreuth, 95447 Bayreuth, Germany**

Lead-free halide double perovskites are promising stable and non-toxic alternatives to methylammonium lead iodide in the field of photovoltaics. In this context, the most commonly used double perovskite is $\text{Cs}_2\text{AgBiBr}_6$, due to its favorable charge transport properties. However, the maximum power conversion efficiency obtained for this material does not exceed 3%, as a consequence of its wide indirect gap and its intrinsic and extrinsic defects. On the other hand, the materials space that arises from the substitution of different elements in the 4 lattice sites of this structure is large and still mostly unexplored. In this work a neural network is used to predict the band gap of double perovskites from an initial space of 7056 structures and select candidates suitable for visible light absorption. Successive hybrid DFT calculations are used to evaluate the thermodynamic stability, the power conversion efficiency and the effective masses of the selected compounds, and to propose novel potential solar absorbers.

I. INTRODUCTION

In the last years, perovskite solar cells have attracted significant attention in the field of photovoltaics, due to their low production cost and high efficiency. The absorber material in these devices is a hybrid organic-inorganic perovskite containing an organic cation (e.g. methylammonium or formamidinium), lead and a halide¹⁻⁵. Methylammonium lead iodide (MAPI) based solar cells were first reported in 2009 with an efficiency of 3.8%⁶ and their performance rapidly increased in the following years. Today, the highest power conversion efficiency for a perovskite solar cell is 25.5%⁷ for formamidinium lead iodide (FAPbI₃) thin films, which is comparable to that of Si single crystal solar cells. These materials possess ideal charge transport properties such as high and balanced carrier mobility and long diffusion length^{8,9}, but the toxicity of Pb and the instability of the structure when exposed to humidity and heat prevent a large scale application of this technology. Several attempts have been made to replace Pb^{2+} with Ge^{2+} or Sn^{2+} , however, the resulting structures have shown poor stability due to the oxidation of Ge and Sn to 4+ formal charge state^{10,11}. Another possible strategy is to substitute two Pb atoms with two cations of charge +1 and +3 in an alternated way, to form the double perovskite structure $\text{A}_2\text{BB}'\text{X}_6$. Some of the most extensively studied halide double perovskites in the field of photovoltaics are $\text{Cs}_2\text{AgBiBr}_6$ ¹²⁻¹⁹ and $\text{Cs}_2\text{AgInCl}_6$ ^{20,21}. However, solar cells based on the former have never reached an efficiency above 3% due to its large indirect gap, while the latter has

a direct gap but the parity-forbidden transition²² makes it a weak absorber. A small direct gap of 0.95 eV was found for $\text{Cs}_2\text{AgTlBr}_6$ ²³ but the high toxicity of Tl limits its application.

Given that double perovskites are quaternary compounds, there are in principle many thousands of possible compositions, with an equally large potential range of optoelectronic properties. Sampling this large design space, though, is not necessarily an easy task even for theory. Considering that accurate predictions of the perovskite electronic structure necessitate computationally expensive theoretical methods such as hybrid functionals and spin-orbit coupling¹³. Earlier studies of perovskites, performing e.g. high-throughput screening,^{24,25} were thus often limited in the employed methods, the search range, or focused only on a subset of properties.

Notable examples here include the works of Filip *et al.*²⁶, Zhao *et al.*²⁷, Volonakis *et al.*²⁸, Roknuzzaman *et al.*²⁹, and Ding *et al.*³⁰, which screened limited search spaces up to a thousand compounds. These studies employed density functional theory at the semi-local, or sometimes at the hybrid level, to also compute the compounds stabilities. Larger studies of up to a few thousand double perovskites,^{31,32} on the other hand, tended to employ geometric arguments³³ to pre-filter the search space.

Recognizing the limits of first-principles calculations, several groups employed machine learning (ML)-based methods to choose potential candidate materials. Unfortunately, such methods tend to also need large amounts of data for their training, which often was generated using comparatively cheap computational methods.

Schmidt *et al.*³⁴ generated a database of almost 250,000 cubic perovskites calculated via DFT with the PBE(+U) functional. Among these, 641 were found to be stable and overall 1562 had a PBE gap above 0.5 eV. This database was also used as benchmark to compare the performance of several ML models (ridge regression, neural networks, random forest, and extremely randomized trees) on the prediction of the energy above hull. The most accurate method was found to be extremely randomized trees. Saidi *et al.*³⁵ used a hierarchical convolutional neural network (CNN) to predict the lattice constant, octahedral angle and band gap of hybrid metal halide perovskites ABX_3 , focusing mainly on the effect of the organic cation A. Li *et al.*³⁶ trained several ML models (gradient tree boosting regression, kernel ridge regression, support vector regression, bootstrap aggregating regression, Gaussian process regression (GPR) and random forest) to predict the formation energy of ABO_3 oxide perovskites and used it as instrumental variable to successively predict the band gap. The models were trained on 1593 oxide perovskites obtained from the Materials Project database³⁷ and resulted in a lowest mean absolute error of 0.384 eV for the GPR model. Paliana *et al.*³⁸ applied kernel ridge regression (KRR) to predict the band gap of oxide double perovskites ($AA'BB'O_6$), starting from a database of 1306 DFT band gaps calculated with the GLLB-SC functional³⁹. In their workflow, they selected 16 elemental features and 16 LASSO-based⁴⁰ compound features to build descriptors to be tested via a linear least square fit (LLSF). Subsequently, they applied KRR on the best-performing ones, obtaining a final root mean squared error (RMSE) of 0.36 eV on a test set including 10% of the structures in the database. Agiorgousis *et al.*⁴¹ trained a random forest algorithm on the band gaps of chalcogenide double perovskites calculated via hybrid DFT using the HSE06 functional to identify promising solar absorbers. The stability of the selected compounds was evaluated by combining information from the geometric Goldschmidt tolerance factor, the decomposition energy and molecular dynamics (MD) simulations. For the stable compounds, optical absorption was calculated, leading to the discovery of 5 promising sulfide double perovskites. In the field of halide double perovskites, Konno⁴² employed a convolutional neural network to implicitly extract elemental features from the position of the atoms in the periodic table. The CNN was trained and tested on a dataset of 3734 experimental band gaps and predicted band gaps with a RMSE of 0.42 eV. Im *et al.*⁴³ used a gradient boosting regression tree (GBRT) to predict the formation energy and the band gap of halide double perovskites, reaching a RMSE of 0.021 eV/atom and 0.223 eV respectively. The model was trained on the DFT data of 540 compounds calculated with the PBE functional. Yang *et al.*⁴⁴ compared the performance of GBRT, ridge regression, support vector regression, KRR, a bagging ensemble algorithm, and a random forest ensemble algorithm and applied GBRT to explore an initial space of 16400 double perovskites.

Following in these footsteps, we here use a convolutional neural network with a periodic table representation (PTR) of the input compounds,⁴⁵ to sample a space of 7056 double perovskites with 2 alkali metals in the position A, 44 metals in the position B/B' and 4 halides in the position X (Figure 1). The PTR has shown to be very useful in any material's discovery situation where the elements of the search space share a similar basic structure, such as Heusler compounds⁴⁵ or, as in our case, double perovskites⁴⁶. It also has the great advantage that no additional computations are necessary to generate⁴². Finally the PTR essentially represents the material as a periodic 2D image and thus lends itself naturally to a treatment by CNNs which were, after all, conceived for image recognition purposes.

In this work we focus on a comprehensive set of properties relevant for photovoltaic applications, the thermodynamic stability of the materials, their power conversion efficiency and the effective masses of their charge carriers.⁴⁷ All our training and test data are computed on the level of hybrid DFT including spin-orbit coupling to ensure a high predictivity of our results. We find a number of promising perovskites not yet considered in experiment, with power conversion efficiencies above 15%. Upon relaxing the criterion of cubic symmetry, we also find a number of perovskite-like structures, with equally high efficiencies but better predicted thermodynamic stabilities.

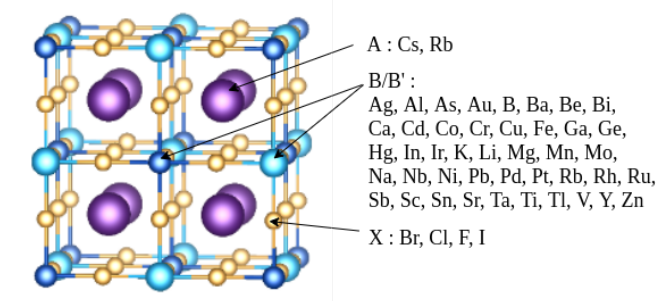


FIG. 1: Double perovskite structure and the compositional space explored

II. METHODS

The training and test sets include 764 and 200 structures, respectively, calculated by DFT using the FHI-aims code⁴⁸. We used the HSE06^{49,50} exchange-correlation functional, a $(4 \times 4 \times 4)$ k-point grid, an energy convergence threshold of 10^{-6} eV and a density convergence threshold of 10^{-6} e/ a_0^3 , where a_0 is a Bohr radius. We use the numeric atom-centered *light* basis sets as implemented in FHI-aims⁴⁸. For most computations, the geometry was optimized in a symmetry-preserving framework, with a convergence threshold for the forces of 10^{-2} eV/Å. The calculations include a non-self-consistent

spin-orbit coupling correction⁵¹ and collinear treatment of the spin, which was initialized following the configuration of isolated atoms. In the structures containing two metals with unpaired electrons, the two spins were initialized in a antiparallel configuration.

The input for the convolutional neural network is a tensor with 3 channels, one for each of the A, B, and X sites. Each channel has the shape of a periodic table filled with zeros and with the stoichiometric coefficient (2 for A, 1 for B and B' and 6 for X) on the position of the four elements in the structure. The neural network (cf. Table I) has 5 convolutional layers with four 2x2 kernels and one 1x2 kernel, and 4 fully connected layers. Each layer has LeakyReLU⁵² as activation function, with a negative slope of 0.2. The fully connected layers include layer normalization⁵³ and dropout⁵⁴ with a probability of 0.25. The network was trained using the Adam optimizer⁵⁵ on batches of 100 samples for 1000 training set iterations, with a learning rate of 0.001, a weight decay of 0.0005 and cosine annealing⁵⁶ as learning rate scheduler. The hyperparameters were chosen in order to minimize the loss between predicted and calculated band gap values on the test set. For the structures with a predicted band gap between 0.9 and 1.6 eV, the thermodynamic stability was estimated by calculating the enthalpy of the decomposition reaction.⁵⁷ For the stable compounds the absorption coefficient was calculated using the random phase approximation on an increased k-point grid density of (8x8x8) and a gaussian broadening of 0.05 eV. From this, the spectroscopic limited maximum efficiency (SLME) was calculated to estimate the maximum theoretical power conversion efficiency, following a method proposed by Yu and Zunger⁵⁸. Additionally, the effective mass was calculated by parabolic fit of the band edges along the high symmetry directions.

Convolutional layers				
Kernel	Channels	Activation	Dropout	Norm
2x2	3,100	LeakyReLU(0.2)	0.25	-
2x2	100,100	LeakyReLU(0.2)	0.25	-
2x2	100,100	LeakyReLU(0.2)	0.25	-
2x2	100,100	LeakyReLU(0.2)	0.25	-
1x2	100,100	LeakyReLU(0.2)	0.25	-
Fully connected layers				
Nodes	Activation	Dropout	Norm	
1200,200	LeakyReLU(0.2)	0.25	layer	
200,200	LeakyReLU(0.2)	0.25	layer	
200,200	LeakyReLU(0.2)	0.25	layer	
200,1	LeakyReLU(0.2)	0.25	layer	

TABLE I: Network architecture

III. RESULTS AND DISCUSSION

The result of the training on a randomly sampled set of 200 structures is shown in Figure 2. With the exception of some outliers the model can predict the band gap with a reasonable accuracy and an overall MAE of 0.21 eV and RMSE of 0.45 eV. The machine learning model is then used to select candidates with a predicted band gap between 0.9 and 1.6 eV. From this set of 459 structures, first those that contain toxic elements have been excluded. Subsequently, the band gap of the remaining 303 structures was explicitly computed at the hybrid DFT level (unless they were already contained in the initial training or test set for the ML model). For the 119 compounds with a DFT band gap included in the same interval, the decomposition enthalpy has been calculated (cf. Figure 3). For a compound to be stable the decomposition enthalpy must be positive, but given the finite accuracy of the employed approximate DFT functional and the fact that the DFT calculations don't include any temperature effect, also the structures with a decomposition enthalpy between -50 and 0 meV/atom have been included in the successive analysis – as candidates potentially stable at room temperature or metastable. As it has been shown by Sun *et al.*⁵⁹, metastable compounds are often found in this energy interval.

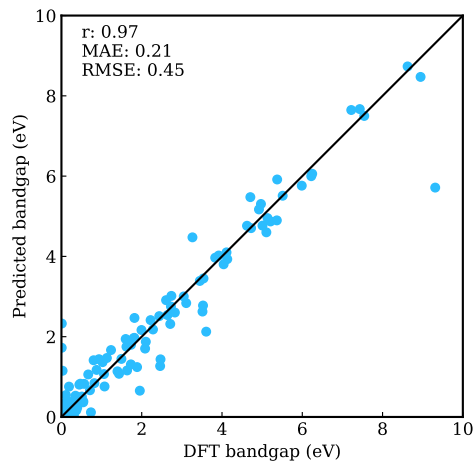


FIG. 2: Training result on a test set of 200 structures

The maximum theoretical power conversion efficiency of the 12 stable and 17 metastable candidates thus identified was calculated for a layer thickness up to 5 μm (see Figure 4 and 5).

The results are summarized in Table II.

Efficiencies above 20% were found for compounds with a dipole-allowed transition in correspondence of their direct or quasi-direct band gap. This is the case for $\text{Cs}_2\text{GeSnCl}_6$ which has a direct gap of 1.41 eV and an efficiency of 28%, for $\text{Cs}_2\text{GeSnBr}_6$, which has a direct gap of 0.95 eV and an efficiency of 23%, and for $\text{Rb}_2\text{CrInI}_6$, with a direct gap at 0.97 eV and a transition at 1.00 eV.

Structure	ΔH_D (meV/at)	E_{gap} (eV)	E_{abs} (eV)	SLME (%)	m_h^* (m_0)		m_e^* (m_0)	
Rb ₂ AgIrBr ₆	-48	1.30	2.03	6	-1.71 (X- Γ)	-3.81 (X-W)	0.34 (X- Γ)	0.31 (X-W)
Cs ₂ CrNaI ₆	-46	0.99	2.20	0	-1.88 (Γ -X)	-0.95 (Γ -L)	0.49 (X- Γ)	0.52 (X-W)
Rb ₂ AgFeBr ₆	-45	1.09	2.31	0	-0.38 (Γ -X)	-0.52 (Γ -L)	0.56 (X- Γ)	0.46 (X-W)
Cs ₂ AlLiI ₆	-44	1.31	1.67	20	-0.81 (Γ -X)	-1.24 (Γ -L)	0.28 (Γ -X)	0.28 (Γ -L)
Rb ₂ CrInI ₆	-43	0.97	1.00	24	-0.42 (L- Γ)	-0.14 (L-W)	0.65 (L- Γ)	0.19 (L-W)
Cs ₂ CuInCl ₆	-38	1.36	1.65	19	* (Γ -X)	-1.06 (Γ -L)	0.27 (Γ -X)	0.27 (Γ -L)
Cs ₂ AgInBr ₆	-36	1.27	1.61	20	-5.62 (Γ -X)	-0.71 (Γ -L)	0.20 (Γ -X)	0.20 (Γ -L)
Rb ₂ AgRhBr ₆	-36	1.49	2.67	2	-1.06 (L- Γ)	-0.69 (L-W)	0.36 (X- Γ)	0.30 (X-W)
Rb ₂ CrGaI ₆	-35	1.19	1.49	20	-1.26 (Γ -X)	-0.86 (Γ -L)	0.66 (L- Γ)	0.26 (L-W)
Rb ₂ AuMoBr ₆	-35	1.26	2.15	4	*	*	*	*
Cs ₂ CrInI ₆	-29	1.03	1.38	11	-0.45 (L- Γ)	-0.15 (L- Γ)	0.66 (L-W)	0.21 (L-W)
Cs ₂ GeSnCl ₆	-28	1.41	1.41	28	-0.13 (Γ -X)	-0.13 (Γ -L)	0.20 (Γ -X)	0.20 (Γ -L)
Cs ₂ GeSnBr ₆	-27	0.95	0.95	23	-0.09 (Γ -X)	-0.09 (Γ -L)	0.14 (Γ -X)	0.14 (Γ -L)
Cs ₂ CrGaI ₆	-26	1.19	1.49	20	-1.22 (Γ -X)	-0.88 (Γ -L)	0.67 (L- Γ)	0.27 (L-W)
Rb ₂ FeRhCl ₆	-9	0.99	1.58	9	-0.39 (L- Γ)	-0.36 (L-W)	1.80 (X- Γ)	0.59 (X-W)
Rb ₂ FeInCl ₆	-4	1.19	1.73	15	-0.29 (X- Γ)	-1.35 (X-W)	27.30 (L- Γ)	8.31 (L-W)
Rb ₂ AgInBr ₆	-2	1.23	1.58	17	-7.39 (Γ -X)	-0.66 (Γ -L)	0.20 (Γ -X)	0.20 (Γ -L)
Rb ₂ CuRuF ₆	6	0.99	1.44	9	-1.15 (Γ -X)	-1.59 (Γ -L)	15.00 (L- Γ)	7.60 (L-W)
Rb ₂ CuFeCl ₆	18	1.26	2.05	7	* (Γ -X)	-0.79 (Γ -L)	0.78 (X- Γ)	0.62 (X-W)
Rb ₂ NiSnI ₆	42	0.92	1.96	0	-0.20 (X- Γ)	-0.99 (X-W)	0.80 (L- Γ)	0.40 (L-W)
Rb ₂ CaNiI ₆	44	1.47	2.33	8	-1.20 (Γ -X)	-0.85 (Γ -L)	0.69 (X- Γ)	0.92 (X-W)
Cs ₂ NiSnI ₆	44	0.96	1.93	0	-0.21 (X- Γ)	-1.09 (X-W)	0.82 (L- Γ)	0.40 (L-W)
Rb ₂ NiSnBr ₆	65	1.56	2.72	2	-0.22 (X- Γ)	-1.18 (X-W)	0.99 (L- Γ)	0.50 (L-W)
Rb ₂ FeKI ₆	76	1.13	2.13	1	-0.17 (Γ -X)	-1.14 (Γ -L)	0.55 (X- Γ)	0.80 (X-W)
Cs ₂ CrScI ₆	77	1.37	1.88	17	-0.87 (L- Γ)	-0.55 (L-W)	0.54 (X- Γ)	0.46 (X-W)
Cs ₂ FeRbI ₆	87	1.24	2.13	5	-1.97 (Γ -X)	-1.46 (Γ -L)	8.25 (X- Γ)	1.17 (X-W)
Cs ₂ FeKI ₆	100	1.14	2.10	2	-1.56 (Γ -X)	-1.21 (Γ -L)	5.72 (X- Γ)	1.63 (X-W)
Cs ₂ MnNbI ₆	246	1.36	2.16	8	*	*	*	*
Cs ₂ GeMnI ₆	322	1.31	2.43	6	-0.22 (X- Γ)	-0.87 (X-W)	0.27 (L- Γ)	0.20 (L-W)

TABLE II: Decomposition enthalpy, DFT band gap, absorption energy, spectroscopic limited maximum power conversion efficiency at 5 μ m and carrier effective masses of the identified metastable and stable compounds, after symmetry constrained geometry optimization. Missing values (*) are due to one or both band edges having bands too narrow to calculate the curvature.

Cs₂GeSnCl₆ and Cs₂GeSnBr₆ also show optimal charge transport properties due to their low and balanced carrier effective masses (-0.13 m_0 and 0.20 m_0 for Cs₂GeSnCl₆, -0.09 m_0 and 0.14 m_0 for Cs₂GeSnBr₆, in units of electron masses m_0 for holes and electrons, respectively).

Rb₂CrInI₆ has heavier and anisotropic effective masses, but still comparable to that of Cs₂AgBiBr₆. Also some materials with indirect gap show a high efficiency, namely Cs₂AlLiI₆, Cs₂CuInCl₆, Cs₂AgInBr₆, Rb₂CrGaI₆ and Cs₂CrGaI₆. However these compounds have negative decomposition enthalpy and might not be stable at room temperature. Additionally, their bands are definitely narrower.

Among the structures with positive decomposition enthalpy, the highest efficiency (17%) was found for Cs₂CrScI₆, with an indirect gap of 1.37 eV and absorption energy of 1.88 eV. The carriers effective masses are of the order of 0.5 m_0 , except for holes along the L- Γ

direction, where m_h^* is -0.87 m_0 .

Finally non symmetry-constrained relaxations show that with a threshold of 0.1 Å the majority of the structures retains the initial cubic spacegroup $Fm-3m$ with the exception of 4 tetragonal structures, namely Rb₂AgIrBr₆ (I_4), Cs₂CuInCl₆ (I_4/mmm), Rb₂CuFeCl₆ (I_4/mmm) and Rb₂CuRuF₆ (I_4/mmm), one monoclinic structure, Cs₂FeRbI₆ ($C2/m$), and one triclinic, Rb₂AuMoBr₆ ($P-1$).

Due to this second relaxation, the decomposition enthalpy of Rb₂AgInBr₆ reaches -0.7 meV/atom and a power conversion efficiency of 17%.

IV. CONCLUSIONS

In this work, we screened a large chemical space (7056 compounds) of inorganic halide double perovskites to un-

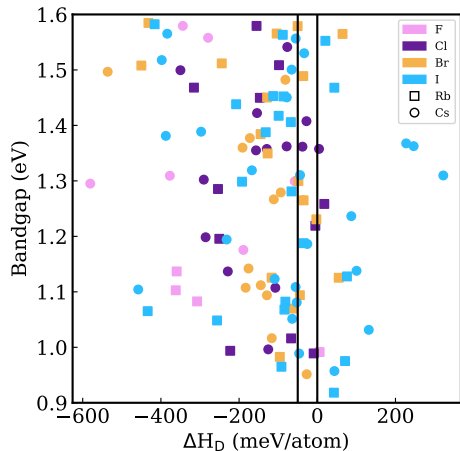


FIG. 3: Enthalpy of the decomposition reaction as a function of DFT band gap. The compounds with $\Delta H_D > 0$ meV/atom are stable, while those included between the vertical lines (from -50 to 0 meV/atom) are assumed to be metastable (see text)

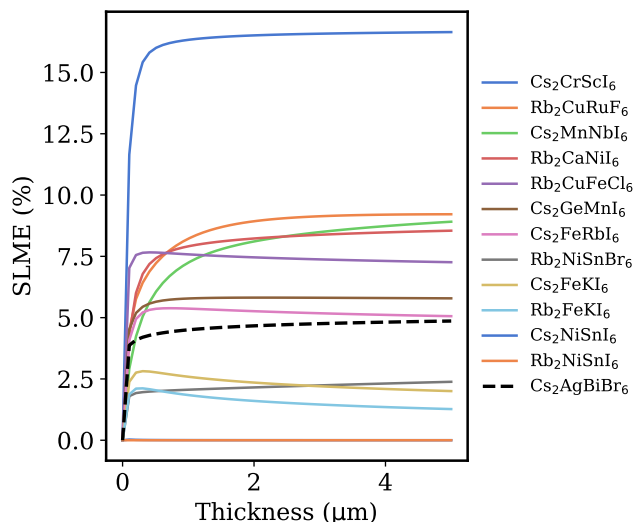


FIG. 4: SLME for stable structures. The efficiency of $\text{Cs}_2\text{AgBiBr}_6$ is shown for comparison

cover suitable candidates for photovoltaic applications. We applied a funnel-type approach to identify a pool of potential candidates and then reduce it by successively performing more demanding calculations based on band gap, thermodynamic stability, power conversion efficiency and carrier effective masses. Thereby we employed a state-of-the-art ML approach as a first step to limit the number of expensive band-structure calculation to just the 964 compounds used in training and testing

the ML model. This is based on a neural network architecture composed of convolutional and fully connected layers with a periodic table representation of the perovskites. This approach yielded a high accuracy for the

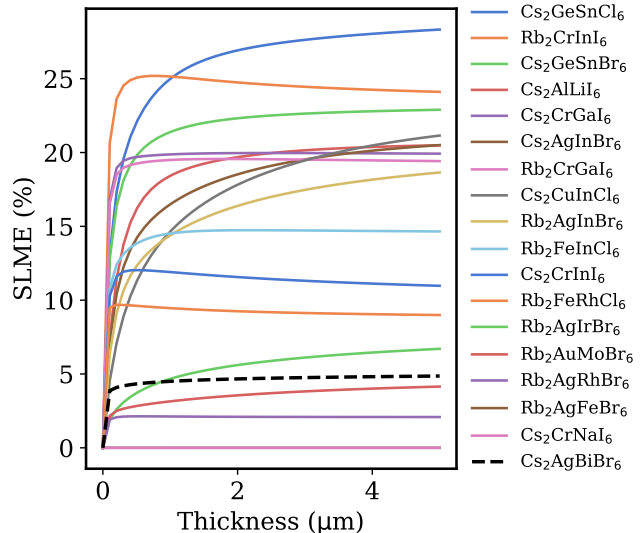


FIG. 5: SLME for metastable structures. The efficiency of $\text{Cs}_2\text{AgBiBr}_6$ is shown for comparison

prediction of band gaps versus DFT results. The latter were all computed using high accuracy hybrid DFT including spin-orbit coupling in order to ensure high predictivity of our results. We find a number of very high performing compounds—with efficiencies as high as 28% and very low carrier effective masses ($-0.13m_0$ for holes and $0.20m_0$ for electrons) for $\text{Cs}_2\text{GeSnCl}_6$. Unfortunately, our calculations show that such high performing compounds might only be meta-stable. Among the compounds predicted to be thermodynamically stable, we still find some with efficiencies of up to 17% ($\text{Rb}_2\text{AgInBr}_6$) albeit with worse and more anisotropic effective masses. Notably, when relaxing the strict requirement of cubic symmetry, we find 6 compounds to achieve higher stabilities at lower symmetries.

Thus, while we do find a few novel materials, trade-offs between power conversion efficiency, carrier mobility and (meta-)stability may indeed be unavoidable for this materials class.

Acknowledgements: This work was supported by the Deutsche Forschungsgemeinschaft (DFG, German Research Foundation) under the priority programme SPP 2196, grant No. RE1509/3701. HO further thanks the DFG for support within the Heisenberg Program, grant No. OB425/9-1.

* harald.oberhofer@uni-bayreuth.de

¹ J. Höcker, F. Brust, M. Armer, V. Dyakonov, *CrystEng-*

Structure	ΔH_D (meV/atom)	E_{gap} (eV)	E_{abs} (eV)	SLME (%)	Spacegroup symbol
Rb ₂ AgIrBr ₆	-32	1.95	2.43	15	I4
Cs ₂ CrNaI ₆	-44	0.99	1.63	8	Fm-3m
Rb ₂ AgFeBr ₆	-43	1.04	2.31	0	Fm-3m
Cs ₂ AlLiI ₆	-42	1.30	1.67	20	Fm-3m
Rb ₂ CrInI ₆	-42	0.91	0.93	23	Fm-3m
Cs ₂ CuInCl ₆	-28	2.21	2.54	12	I4/mmm
Cs ₂ AgInBr ₆	-34	1.22	1.58	18	Fm-3m
Rb ₂ AgRhBr ₆	-33	1.45	2.27	8	Fm-3m
Rb ₂ CrGaI ₆	-34	1.19	1.47	19	Fm-3m
Rb ₂ AuMoBr ₆	6	2.69	3.27	4	P-1
Cs ₂ CrInI ₆	-28	0.97	1.00	24	Fm-3m
Cs ₂ GeSnCl ₆	-27	1.35	1.35	27	Fm-3m
Cs ₂ GeSnBr ₆	-26	0.89	0.90	21	Fm-3m
Cs ₂ CrGaI ₆	-24	1.21	1.48	21	Fm-3m
Rb ₂ FeRhCl ₆	-8	0.93	1.54	10	Fm-3m
Rb ₂ AgInBr ₆	-0.7	1.20	1.57	17	Fm-3m
Rb ₂ FeInCl ₆	-4	1.06	1.61	14	Fm-3m
Rb ₂ CuRuF ₆	7	0.91	1.40	6	I4/mmm
Rb ₂ CuFeCl ₆	19	1.13	2.10	4	I4/mmm
Rb ₂ NiSnI ₆	43	0.87	1.97	0	Fm-3m
Rb ₂ CaNiI ₆	44	1.48	2.35	8	Fm-3m
Cs ₂ NiSnI ₆	45	0.92	1.94	0	Fm-3m
Rb ₂ NiSnBr ₆	66	1.51	2.72	1	Fm-3m
Rb ₂ FeKI ₆	77	1.13	2.15	1	Fm-3m
Cs ₂ CrScI ₆	79	1.37	1.88	17	Fm-3m
Cs ₂ FeRbI ₆	105	1.40	2.13	11	C2/m
Cs ₂ FeKI ₆	102	1.14	2.13	2	Fm-3m
Cs ₂ MnNbI ₆	248	1.41	2.17	9	Fm-3m
Cs ₂ GeMnI ₆	323	1.29	2.43	6	Fm-3m

TABLE III: Decomposition enthalpy, DFT band gap, absorption energy, spectroscopic limited maximum power conversion efficiency at 5 μm of the metastable and stable compounds, after non symmetry constrained geometry optimization

Comm **2021**, *23*, 2202–2207.

- ² A. Biewald, N. Giesbrecht, T. Bein, P. Docampo, A. Hartschuh, R. Ciesielski, *ACS Applied Materials & Interfaces* **2019**, *11*, 20838–20844.
- ³ A. M. Leguy, Y. Hu, M. Campoy-Quiles, M. I. Alonso, O. J. Weber, P. Azarhoosh, M. Van Schilfgaarde, M. T. Weller, T. Bein, J. Nelson *et al.*, *Chemistry of Materials* **2015**, *27*, 3397–3407.
- ⁴ W. Tress, *Advanced Energy Materials* **2017**, *7*, 1602358.
- ⁵ Y. Zhao, K. Zhu, *Chemical Society Reviews* **2016**, *45*, 655–689.
- ⁶ A. Kojima, K. Teshima, Y. Shirai, T. Miyasaka, *Journal of the American Chemical Society* **2009**, *131*, 6050–6051.
- ⁷ M. Green, E. Dunlop, J. Hohl-Ebinger, M. Yoshita, N. Kopidakis, X. Hao, *Progress in Photovoltaics: Research and Applications* **2021**, *29*, 3–15.
- ⁸ Y. Bi, E. M. Hutter, Y. Fang, Q. Dong, J. Huang, T. J.

- Savenije, *The Journal of Physical Chemistry Letters* **2016**, *7*, 923–928.
- ⁹ T. Dittrich, F. Lang, O. Shargaieva, J. Rappich, N. Nickel, E. Unger, B. Rech, *Applied Physics Letters* **2016**, *109*, 073901.
 - ¹⁰ Y. Ogomi, A. Morita, S. Tsukamoto, T. Saitho, N. Fujikawa, Q. Shen, T. Toyoda, K. Yoshino, S. S. Pandey, T. Ma *et al.*, *The Journal of Physical Chemistry Letters* **2014**, *5*, 1004–1011.
 - ¹¹ N. K. Noel, S. D. Stranks, A. Abate, C. Wehrenfennig, S. Guarnera, A.-A. Haghighirad, A. Sadhanala, G. E. Eperon, S. K. Pathak, M. B. Johnston *et al.*, *Energy & Environmental Science* **2014**, *7*, 3061–3068.
 - ¹² G. Volonakis, M. R. Filip, A. A. Haghighirad, N. Sakai, B. Wenger, H. J. Snaith, F. Giustino, *The Journal of Physical Chemistry Letters* **2016**, *7*, 1254–1259.
 - ¹³ M. R. Filip, S. Hillman, A. A. Haghighirad, H. J. Snaith, F. Giustino, *The Journal of Physical Chemistry Letters* **2016**, *7*, 2579–2585.
 - ¹⁴ A. H. Slavney, L. Leppert, D. Bartesaghi, A. Gold-Parker, M. F. Toney, T. J. Savenije, J. B. Neaton, H. I. Karunadasa, *Journal of the American Chemical Society* **2017**, *139*, 5015–5018.
 - ¹⁵ E. T. McClure, M. R. Ball, W. Windl, P. M. Woodward, *Chemistry of Materials* **2016**, *28*, 1348–1354.
 - ¹⁶ D. Bartesaghi, A. H. Slavney, M. C. Gélvez-Rueda, B. A. Connor, F. C. Grozema, H. I. Karunadasa, T. J. Savenije, *The Journal of Physical Chemistry C* **2018**, *122*, 4809–4816.
 - ¹⁷ M. T. Sirtl, M. Armer, L. K. Reb, R. Hooijer, P. Dörflinger, M. A. Scheel, K. Tvingstedt, P. Rieder, N. Glück, P. Pandit, S. V. Roth, P. Müller-Buschbaum, V. Dyakonov, T. Bein, *ACS Applied Energy Materials* **2020**, *3*, 11597–11609.
 - ¹⁸ X. Yang, Y. Chen, P. Liu, H. Xiang, W. Wang, R. Ran, W. Zhou, Z. Shao, *Advanced Functional Materials* **2020**, *30*, 2001557.
 - ¹⁹ M. Armer, J. Höcker, C. Büchner, S. Häfele, P. Dörflinger, M. T. Sirtl, K. Tvingstedt, T. Bein, V. Dyakonov, *CrystrEngComm* **2021**, *23*, 6848–6854.
 - ²⁰ J. Luo, S. Li, H. Wu, Y. Zhou, Y. Li, J. Liu, J. Li, K. Li, F. Yi, G. Niu *et al.*, *ACS Photonics* **2018**, *5*, 398–405.
 - ²¹ J. C. Dahl, W. T. Osowiecki, Y. Cai, J. K. Swabeck, Y. Bekenstein, M. Asta, E. M. Chan, A. P. Alivisatos, *Chemistry of Materials* **2019**, *31*, 3134–3143.
 - ²² W. Meng, X. Wang, Z. Xiao, J. Wang, D. B. Mitzi, Y. Yan, *The Journal of Physical Chemistry Letters* **2017**, *8*, 2999–3007.
 - ²³ A. H. Slavney, L. Leppert, A. Saldivar Valdes, D. Bartesaghi, T. J. Savenije, J. B. Neaton, H. I. Karunadasa, *Angewandte Chemie International Edition* **2018**, *57*, 12765–12770.
 - ²⁴ R. Jacobs, G. Luo, D. Morgan, *Advanced Functional Materials* **2019**, *29*, 1804354.
 - ²⁵ S. X. Tao, X. Cao, P. A. Bobbert, *Scientific Reports* **2017**, *7*, 1–9.
 - ²⁶ M. R. Filip, X. Liu, A. Miglio, G. Hautier, F. Giustino, *The Journal of Physical Chemistry C* **2018**, *122*, 158–170.
 - ²⁷ X.-G. Zhao, J.-H. Yang, Y. Fu, D. Yang, Q. Xu, L. Yu, S.-H. Wei, L. Zhang, *Journal of the American Chemical Society* **2017**, *139*, 2630–2638.
 - ²⁸ G. Volonakis, A. A. Haghighirad, H. J. Snaith, F. Giustino, *The Journal of Physical Chemistry Letters* **2017**, *8*, 3917–3924.

- ²⁹ M. Roknuzzaman, C. Zhang, K. K. Ostrikov, A. Du, H. Wang, L. Wang, T. Tesfamichael, *Scientific Reports* **2019**, *9*, 1–7.
- ³⁰ X.-L. Ding, Z. Gao, G. Mao, S. Chen, Y. Bai, P. Gao, I. D. Gates, C. Wu, W. Yang, J. Yao, *Physical Chemistry Chemical Physics* **2022**, *24*, 3460.
- ³¹ Y. Cai, W. Xie, Y. T. Teng, P. C. Harikesh, B. Ghosh, P. Huck, K. A. Persson, N. Mathews, S. G. Mhaisalkar, M. Sherburne *et al.*, *Chemistry of Materials* **2019**, *31*, 5392–5401.
- ³² C. J. Bartel, J. M. Clary, C. Sutton, D. Vigil-Fowler, B. R. Goldsmith, A. M. Holder, C. B. Musgrave, *Journal of the American Chemical Society* **2020**, *142*, 5135–5145.
- ³³ C. J. Bartel, C. Sutton, B. R. Goldsmith, R. Ouyang, C. B. Musgrave, L. M. Ghiringhelli, M. Scheffler, *Science Advances* **2019**, *5*, eaav0693.
- ³⁴ J. Schmidt, J. Shi, P. Borlido, L. Chen, S. Botti, M. A. Marques, *Chemistry of Materials* **2017**, *29*, 5090–5103.
- ³⁵ W. A. Saidi, W. Shadid, I. E. Castelli, *npj Computational Materials* **2020**, *6*, 1–7.
- ³⁶ C. Li, H. Hao, B. Xu, G. Zhao, L. Chen, S. Zhang, H. Liu, *Journal of Materials Chemistry C* **2020**, *8*, 3127–3136.
- ³⁷ A. Jain, S. P. Ong, G. Hautier, W. Chen, W. D. Richards, S. Dacek, S. Cholia, D. Gunter, D. Skinner, G. Ceder *et al.*, *APL Materials* **2013**, *1*, 011002.
- ³⁸ G. Pilia, A. Mannodi-Kanakithodi, B. Uberuaga, R. Ramprasad, J. Gubernatis, T. Lookman, *Scientific Reports* **2016**, *6*, 1–10.
- ³⁹ M. Kuisma, J. Ojanen, J. Enkovaara, T. T. Rantala, *Physical Review B* **2010**, *82*, 115106.
- ⁴⁰ L. J. Nelson, G. L. Hart, F. Zhou, V. Ozoliņš *et al.*, *Physical Review B* **2013**, *87*, 035125.
- ⁴¹ M. Agiorgousis, Y.-Y. Sun, D.-H. Choe, D. West, S. Zhang, *Advanced Theory and Simulations* **2019**, *2*, 1800173.
- ⁴² T. Konno, *Journal of the Physical Society of Japan* **2020**, *89*, 124006.
- ⁴³ J. Im, S. Lee, T.-W. Ko, H. W. Kim, Y. Hyon, H. Chang, *npj Computational Materials* **2019**, *5*, 1–8.
- ⁴⁴ Z. Yang, Y. Liu, Y. Zhang, L. Wang, C. Lin, Y. Lv, Y. Ma, C. Shao, *The Journal of Physical Chemistry C* **2021**, *125*, 22483.
- ⁴⁵ X. Zheng, P. Zheng, R.-Z. Zhang, *Chemical science* **2018**, *9*, 8426–8432.
- ⁴⁶ T. Konno, H. Kurokawa, F. Nabeshima, Y. Sakishita, R. Ogawa, I. Hosako, A. Maeda, *Phys. Rev. B* **2021**, *103*, 014509.
- ⁴⁷ C. Muschielok, H. Oberhofer, *The Journal of Chemical Physics* **2019**, *151*, 015102.
- ⁴⁸ V. Blum, R. Gehrke, F. Hanke, P. Havu, V. Havu, X. Ren, K. Reuter, M. Scheffler, *Computer Physics Communications* **2009**, *180*, 2175–2196.
- ⁴⁹ J. Heyd, G. E. Scuseria, M. Ernzerhof, *The Journal of Chemical Physics* **2003**, *118*, 8207–8215.
- ⁵⁰ A. V. Krukau, O. A. Vydrov, A. F. Izmaylov, G. E. Scuseria, *The Journal of Chemical Physics* **2006**, *125*, 224106.
- ⁵¹ W. P. Huhn, V. Blum, *Physical Review Materials* **2017**, *1*, 033803.
- ⁵² A. L. Maas, A. Y. Hannun, A. Y. Ng *et al.*, *Proc. icml*, **2013**, p. 3.
- ⁵³ J. L. Ba, J. R. Kiros, G. E. Hinton, *arXiv preprint arXiv:1607.06450* **2016**.
- ⁵⁴ G. E. Hinton, N. Srivastava, A. Krizhevsky, I. Sutskever, R. R. Salakhutdinov, *arXiv preprint arXiv:1207.0580* **2012**.
- ⁵⁵ D. P. Kingma, J. Ba, *arXiv preprint arXiv:1412.6980* **2014**.
- ⁵⁶ I. Loshchilov, F. Hutter, *arXiv preprint arXiv:1608.03983* **2016**.
- ⁵⁷ W. Pu, W. Xiao, J.-W. Wang, X.-W. Li, L. Wang, *Mater. Des.* **2021**, *198*, 109387.
- ⁵⁸ L. Yu, A. Zunger, *Physical Review Letters* **2012**, *108*, 068701.
- ⁵⁹ W. Sun, S. T. Dacek, S. P. Ong, G. Hautier, A. Jain, W. D. Richards, A. C. Gamst, K. A. Persson, G. Ceder, *Science Advances* **2016**, *2*, e1600225.